An FTIR–ATR Investigation of *In Vivo* Poly(ether urethane) Degradation

Y. WU,[1] C. SELLITTI,[1] J. M. ANDERSON,[1] A. HILTNER,[1]* G. A. LODOEN,[2] and C. R. PAYET[3]

[1]Departments of Macromolecular Science and Pathology, Case Western Reserve University, Cleveland, Ohio 44106, [2]E. I. du Pont de Nemours & Company, Inc., Waynesboro, Virginia 22980, and [3]E. I. du Pont de Nemours & Company, Inc., Wilmington, Delaware 19880

SYNOPSIS

Surface degradation of implanted poly(ether urethane)s was studied quantitatively with a micro-ATR–FTIR technique. Substantial degradation was observed particularly in the soft segment at the α-carbon adjacent to the ether linkage. The degradation caused changes in the concentration profiles of the soft-segment groups in the depth direction, and the affected depth was up to 10 microns after implantation for 10 weeks. Inhibition of degradation by antioxidants indicated the oxidative nature of degradation. An *in vivo* poly(ether urethane) degradation mechanism was proposed.

INTRODUCTION

Polyurethanes (PEUs) have found a wide range of biomedical applications because of their combination of physical and chemical properties coupled with their biocompatibility. They have been studied as artificial heart diaphragms, ventricular assist bladders, A–V shunts, vascular grafts, mammary protheses, pacemaker leads, leaflet valves, cardiac patches, and other devices.[1] Polyurethanes, particularly those derived from a polyether soft segment, can be stable in dry and wet conditions for many years[2] and yet when implanted may undergo rapid pitting and cracking. Failure of some PEU cardiac pacing leads has been attributed to autooxidation of soft-segment ether, initiated and propagated by metallic components containing cobalt specifically. Other metals were found to be ineffective in catalyzing the degradation.[3]

The *in vivo* degradation of PEUs can also occur under conditions where cobalt catalysis is not a factor. A previous study of cage-implanted PEU films examined the effect of certain stabilizers on surface cracking and pitting.[4] Cracking inevitably occurred in the PEU samples that did not contain the antioxidant, Santowhite powder, whereas pitting was associated with leaching of one of the additives, Methacrol 2138F. Further studies[5] showed that cracking occurred almost exclusively in the areas covered by foreign body giant cells, indicating that the cracking was due to surface attack by the activated cells. Oxidative degradation of PEUs *in vivo* has been suggested,[6] although the mechanism, and particularly the role of activated cells, has not been clarified.

The FTIR technique can be a powerful tool for characterizing PEU surfaces,[7–10] especially when combined with attenuated total reflection (ATR–FTIR).[11–15] However, ATR–FTIR has not been used to quantitatively study the biodegradation of PEUs, perhaps because the chemical changes are too slight for ready detection with the normal ATR technique. Implantation of PEU specimens produces heterogeneous surfaces characterized by the presence of cloudy and clear areas; in this case, where degradation is a highly localized phenomenon, neither transmission infrared spectroscopy nor conventional attenuated total reflection infrared spectroscopy is satisfactory. With transmission FTIR, small surface changes can be veiled by the unaffected thick bulk region, whereas with the conventional ATR–FTIR, where a relatively large specimen area of about 50 mm^2 is required, the degradation phenomena can be diluted by sampling both cloudy and clear areas. For

* To whom correspondence should be addressed.

Journal of Applied Polymer Science, Vol. 46, 201–211 (1992)
 CCC 0021-8995/92/020201-11$04.00

this reason, micro-ATR–FTIR was used to investigate the chemical degradation of cage-implanted PEU specimens. This technique requires specimens with only a few square millimeters of surface. The same specimens used previously in morphological studies[4] were characterized with the aim of elucidating *in vivo* PEU degradation mechanisms.

EXPERIMENTAL

Poly(ether urethane)s (PEUs), provided by E. I. du Pont Co., were prepared from MDI and poly(tetramethylene glycol) (PTMEG) (MW = 2000) in an approximately 1.6 to 1 capping ratio and chain extended primarily with ethylenediamine. In addition to the base PEU, identified as Sample A, three other PEUs with different additives were also studied. They were identified as Sample B, the base PEU plus 1% of Santowhite; Sample C, the base PEU plus 5% Methacrol 2138F; and Sample D, the base PEU plus 1% Santowhite and 5% Methacrol 2138F.

The PEUs were solution-cast on Mylar polyester substrate from *N,N*-dimethylacetamide with the film thickness of 0.2 mm. The PEU films, cut into approximately 2.5 × 2.5 cm pieces and stripped off the Mylar substrate, were put into stainless-steel wire mesh cages that measured 3.5 cm in length and 1 cm in diameter with the Mylar side facing the cage. The cage specimens were sterilized with ethylene oxide and implanted subcutaneously in the backs of 3-month-old female Sprague-Dawley rats. The specimens were retrieved after 10 weeks, and the cell debris was washed off following the procedures described previously.[4] The specimens were then dried in air for at least 1 day and *in vacuo* at ambient temperature for 48 h and subsequently stored in a darkened desiccator.

The cleaned specimens were coated with 60 Å of gold and examined in the JEOL LSM840A scanning electron microscope (SEM). Attenuated total reflection FTIR spectra were taken with either a BioRad FTS-40 or a Nicolet 800 spectrometer using the micro-ATR attachment made by Harrick Scientific, Inc., that featured two 4× beam condensers and continuous beam angle variation. The ATR internal reflection elements (IRE) used were germanium with 60°, 45°, and 30° endface angles and KRS-5 with 60° and 45° endface angles. A deconvolution program[16] was utilized to distinguish between specific infrared absorptions occurring in the same frequency range. The peak positions assigned in the deconvolution program were determined from the minima of the second derivative spectrum of the infrared region of interest.

RESULTS

The implanted PEUs visually appeared to be cloudy after the cells were removed, and some were opaque in focal areas. Transmission optical micrographs at low magnification qualitatively showed differences in appearance of the four samples. Before implantation, Samples A and B were clear and transparent, but after implantation, areas of fiberlike opaqueness appeared that reduced the transparency and gave the films a cloudy appearance. After 10 weeks implantation, about 70–80% of the area of sample A was affected. The effect was much less on Sample B, and after 10 weeks implantation, only about 30–40% of the area had the fiberlike opaqueness resembling that of Sample A. The SEM micrographs in Figure 1 were representative of the cloudy areas of the implanted PEU films; areas that remained clear after implantation retained the featureless surface morphology of the original PEU films. The cloudiness of Sample A was caused by a dense network of microcracks [Fig. 1(a)]. Rough areas were also observed where cracking appeared to have been sufficiently severe that a surface layer had flaked off. The cloudy areas of implanted Sample B had an overall surface roughness shown in Figure 1b, but there was no evidence of the microcracking and subsequent loss of material from the surface that were characteristic of Sample A.

Films of Samples C and D were initially less transparent than of A and B and, after implantation, were characterized by a diffuse cloudiness rather than fiberlike opaqueness described for A and B. The largest effects of implantation were exhibited by Sample C; more than 90% of the area was affected after 10 weeks implantation. In comparison, only about 30–40% of the area of Sample D was affected and, qualitatively, the cloudiness was less dense than on Sample C. The surface of implanted Sample C was characterized by numerous small pits about 1 μm in diameter [Fig. 1(c)]. A network of microcracks with some flaking of a surface layer appeared superimposed on the pitting. Pitting was also observed on Sample D [Fig. 1(d)], but neither microcracking nor flaking was observed.

The infrared spectrum of unimplanted Sample A (curve a) is compared in Figure 2 with those of the clear (curve b) and cloudy (curve c) areas of Sample

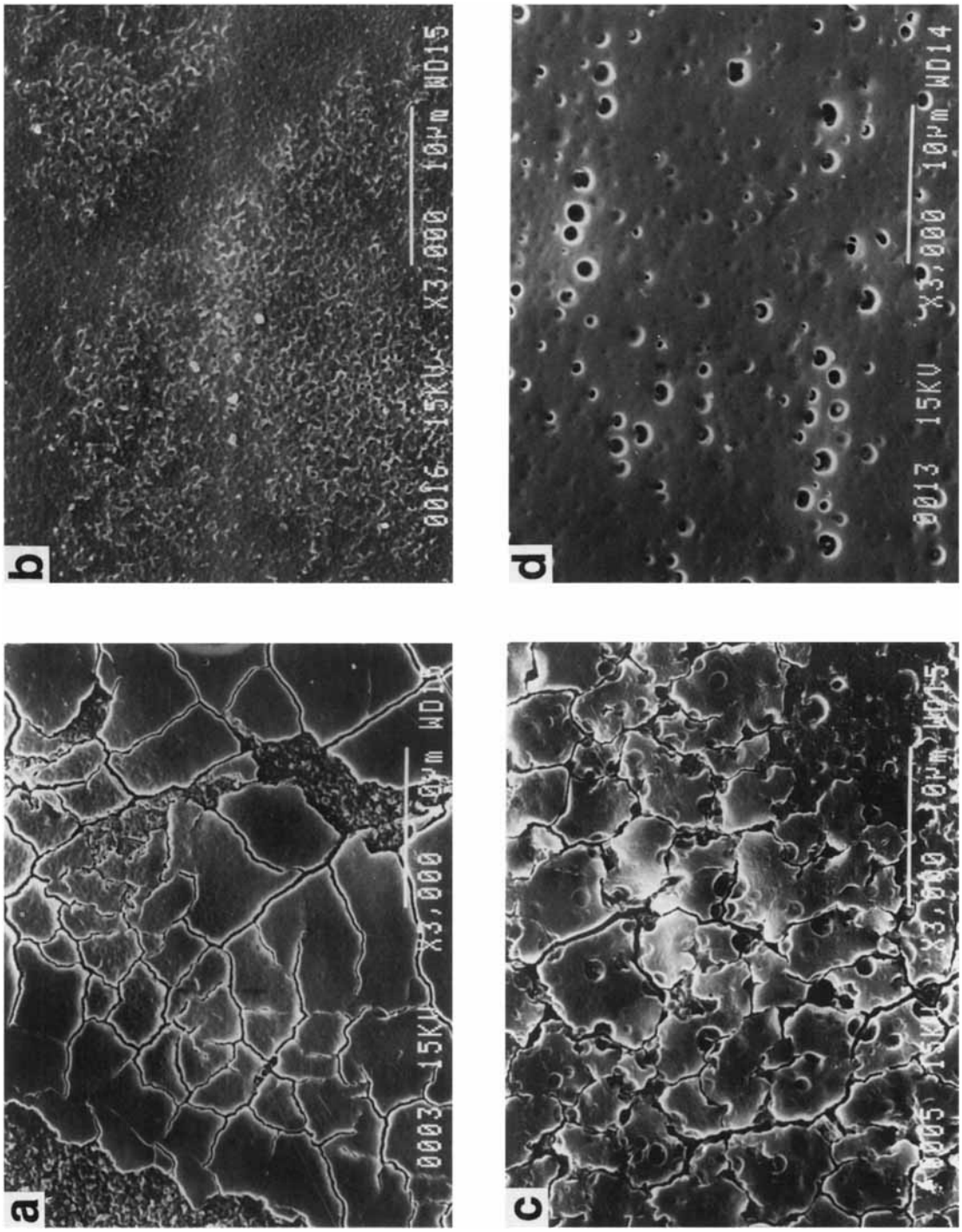

Figure 1 SEM micrographs of implanted PEU samples from the most cloudy areas: (a) Sample A; (b) Sample B; (c) Sample C; (d) Sample D.

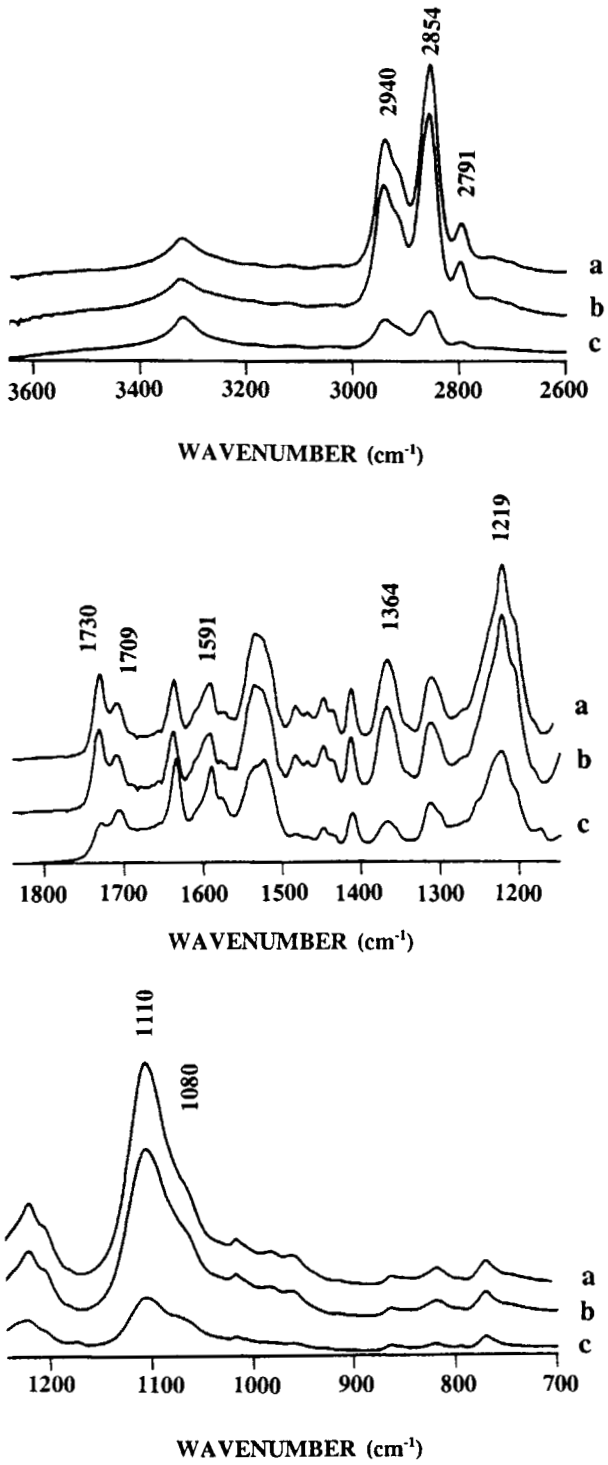

Figure 2 Typical ATR–FTIR spectra of Sample A: (a) unimplanted sample; (b) a clear area of the implanted sample; (c) a cloudy area of the implanted sample.

A implanted for 10 weeks. The spectrum of the clear area did not show any significant differences from the unimplanted one, whereas large intensity changes were observed in the spectrum of the cloudy area, suggesting that chemical degradation occurred primarily in the cloudy areas. The most significant changes were decreases in the methylene bands from the PTMEG soft segment in the region 2940–2790 cm^{-1} and at 1364 cm^{-1}. The absorptions at 1730 and 1709 cm^{-1} due to the urethane carbonyl also decreased. In addition to the bands that decreased, the spectrum contained numerous new absorptions attributed to degradation products such as the bands at 1255, 1174, and 930 cm^{-1}. The major changes in the spectrum and the band assignments are summarized in Table I.

The ATR technique also allowed the depth profiles to be analyzed through the utilization of optical elements with different refractive indices as well as different angles of the incident infrared beam.[20] Infrared spectra of Sample A unimplanted and after 10 weeks implantation are presented in Figure 3. The depth penetration of the infrared beam decreased from curve a to curve c. The spectra of the unimplanted sample did not show any significant depth dependency, whereas those of the cloudy area did. Spectra with less penetration depth showed greater changes from the unimplanted control spectra than those with higher penetration depth. This observation, that spectral features of the implanted sample recorded with the smallest penetration depth differed the most from those of the unimplanted sample, indicated that degradation was a surface phenomenon.

DISCUSSION

Depth Profile Analysis

Spectra such as those in Figure 3 were used to determine the concentration gradients of the individual functional groups in the depth direction in the implanted PEU samples. The relationship between concentration profile, $C(x)$, and the ATR absorbance, A, is given by Harrick[21] as

$$A = \frac{2d_e\epsilon}{d_p}\int_0^\infty C(x)e^{-2x/d_p}\,dx \qquad (1)$$

where $d_e = (n_{21}E_0^2 d_p)/(2\cos\theta)$; E_0, the electric field strength; θ, the incident angle of the IR beam; $n_{21} = n_2/n_1$, with n_1 and n_2 being the refractive indices of the ATR substrate and the polymer film (for PEU $n_2 = 1.5$ was used); ϵ, the extinction coefficient of the band with wavelength λ; and $d_p = [\lambda/(2\pi n_1)][\sin^2\theta - n_{21}^2]^{-1/2}$. However, the function

Table I Assignments of the Major Absorbances in the IR Spectra of Implanted PEUs

	Bands that Decreased
2940 cm^{-1}	$\nu_a(CH_2)$ of β-methylene from PTMEG[7,8,17]
2854 cm^{-1}	$\nu_s(CH_2)$ of β-methylene and $\nu_a(CH_2)$ of α-methylene from PTMEG[7,8,17]
2791 cm^{-1}	$\nu_s(CH_2)$ of α-methylene from PTMEG[7,8,17]
1730 cm^{-1}	$\nu(C{=}O)$ of non-H-bonded carbonyl from urethane[8]
1709 cm^{-1}	$\nu(C{=}O)$ of H-bonded carbonyl from urethane[8]
1364 cm^{-1}	$\omega(CH_2)$ from PTMEG[8,17]
1219 cm^{-1}	$\delta(N{-}H) + \nu(C{-}N)$ of amide III from urea and urethane[7-9]
1110 cm^{-1}	$\nu(C{-}O{-}C)$ of ether from PTMEG[8,9]
1080 cm^{-1}	$\nu(C{-}O{-}C)$ of $CO{-}O{-}C$ from urethane[8]
	New Bands
~3500 cm^{-1}	$\nu(O{-}H)$ of $-CH_2OH$[18,19]
1670 cm^{-1}	$\nu(C{=}O)$ of $-COOH$[18,19]
1300 cm^{-1}	$\nu_a(O{-}C{-}O)$ of $-COOH$[18,19]
1255 cm^{-1}	$\nu(C{-}O)$ of $-CH_2OH$[18,19]
1174 cm^{-1}	$\nu(O{-}C{-}O)$ of $-COOH$ or $CO{-}O{-}CH_2$[18,19]
930 cm^{-1}	$\omega(O{-}C{-}O)$ of $-COOH$[18,19]

ν, stretching; ν_a, asymmetric stretching; ν_s, symmetric stretching; ω, wagging; and δ, bending.

$C(x)$ cannot be readily obtained from experimental data using this equation. Generally, to resolve $C(x)$ it is necessary either to use the Laplacian transform or to assume a specific functional form of $C(x)$. In the latter case, integration of eq. (1) gives a relationship that can be used with experimental data to test the form of $C(x)$ and to obtain characteristic parameters.

Tompkins[22] used step functions for $C(x)$ to model the concentration profiles of oxidized polypropylene films. Carlsson and Wiles[23] used exponential functions to describe the concentration profiles in corona-treated polypropylene. In this study, the latter approach was adopted and exponential functions were used to represent the concentration profiles of the different functional groups. Thus, for groups that decreased after implantation,

$$C(x) = C_\infty(1 - e^{-\delta x}) \tag{2}$$

where C_∞ is the bulk concentration in the sample and δ is a parameter that reflects how rapidly the concentration changes in the depth direction x. The larger δ is, the more rapidly $C(x)$ approaches C_∞ in the depth direction. Substitution of eq. (2) into eq. (1) gives

$$A = d_e \epsilon C_\infty \left[\frac{\delta}{\delta + 2\gamma}\right] \tag{3}$$

where $\gamma = 1/d_p$. However, since d_e depends on experimental conditions, for example, the contact between specimen and the internal reflection element, eq. (3) has to be normalized to a reference band that does not change in intensity. For a band with no change in concentration through the depth,

$$C(x) = \mathbf{C} \tag{4}$$

where $\mathbf{C}$ is a constant representing the average concentration of this group. Then, substitution of eq. (4) into eq. (1) gives

$$A_r = (d_e \epsilon \mathbf{C})_r \tag{5}$$

Finally, ratioing eqs. (3) and (5) and rearranging

$$\left(\frac{A}{A_r}\right)^{-1} = \frac{1}{K} + \frac{2}{\delta K}\gamma \tag{6}$$

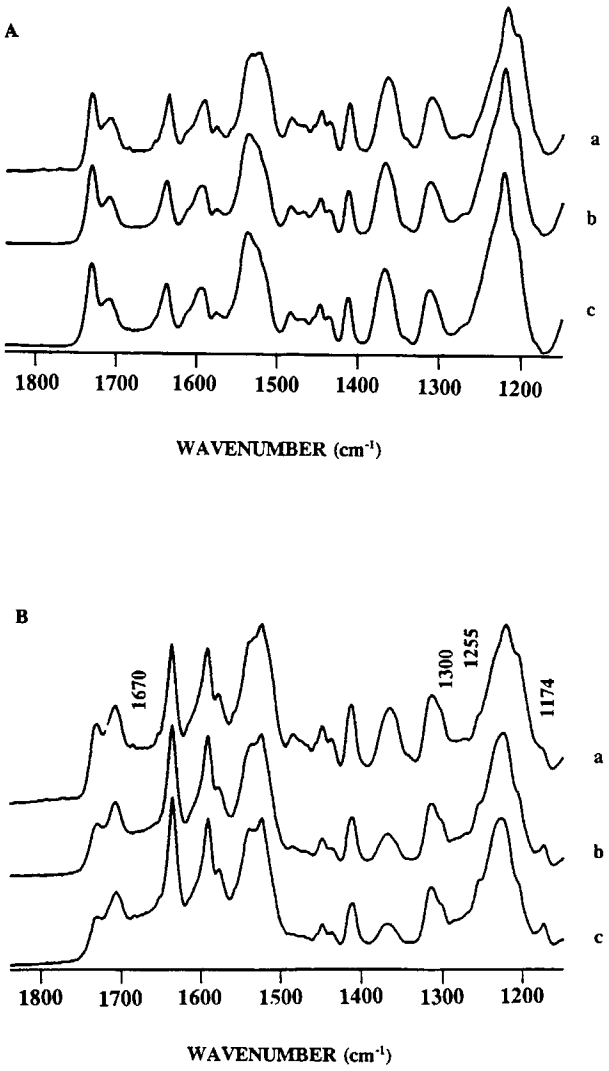

Figure 3 Comparison of ATR–FTIR spectra with different sampling depths: (A) unimplanted Sample A; (B) implanted Sample A in a cloudy area. The sampling depth increased from c to a. Spectrum a was obtained with KRS-5 45° endface angle and 45° incident angle of IR beam; spectrum b was with Ge 45° endface angle and 30° incident angle of IR beam; and spectrum c was with Ge 60° endface angle and 45° incident angle of IR beam.

where

$$K = \frac{d_e \epsilon C_\infty}{(d_e \epsilon \mathbf{C})_r} \qquad (7)$$

A plot of the measured $(A/A_r)^{-1}$ as a function of γ (or d_p^{-1}) should be linear and the parameters δ and K can be evaluated from the slope and the intercept.

Depth Profiles of PEU Samples

The absorption at 1591 cm^{-1} associated to the C=C stretching of the phenyl ring was used as the internal reference. A typical plot of $(A/A_r)^{-1}$ as a function of d_p^{-1} in Figure 4, where the ratio of the absorptions at 1364 and 1591 cm^{-1} for the implanted PEU is compared with the unimplanted sample, showed a good fit of the assumed model with the experimental data. The virtually zero slope of the unimplanted sample meant a very large value of δ and a practically constant concentration in the depth direction. This result was similar to that of Sung and Hu[11] where only moderate change in the soft segment content was found in the depth direction of the Biomer film. The plot of data from the implanted sample was linear with the same intercept as that of the unimplanted sample. The intercept of the plot is related to K, and, from eq. (7), the K value of the implanted sample should be same as that of the unimplanted sample, since if degradation occurred only at the surface, both samples would have the same value of C_∞ in the bulk region. From the slope of the plot, δ was obtained.

Table II lists the δ values of some bands assigned to the soft segment, the linkage region between hard and soft segments, and the hard segment in a cloudy area of the implanted Sample A together with the linear regression coefficients. The ether bands at 1110 cm^{-1} were not analyzed since several absorptions overlapped in this region and it was difficult to measure the absorbance of individual bands quantitatively even with the deconvolution method. The K values reported in the table were averages from the unimplanted Samples A, B, C, and D. The relatively high values of the linear regression coef-

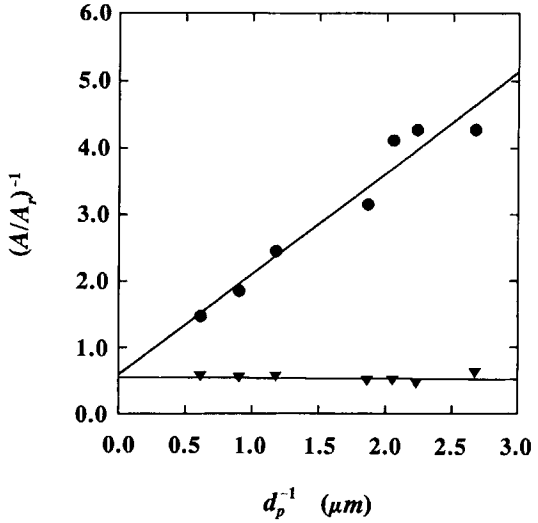

Figure 4 Plot of $(A/A_r)^{-1}$ vs. d_p^{-1} for the methylene band at 1364 cm^{-1}: (●) cloudy area of implanted Sample A; (▼) unimplanted Sample A.

Table II δ Values for Bands that Decreased in Intensity from the Bulk toward the Surface from a Frosty Area of Implanted Sample A

	Band (cm^{-1})						
	Soft Segment				Linkage Region		Hard Segment
	2791	1364	2854	2940	1730	1709	1219
Linear regression coefficient	0.979	0.971	0.994	0.991	0.989	0.977	0.903
K	1.6 ± 0.3	1.9 ± 0.1	4.9 ± 0.2	2.0 ± 0.1	2.0 ± 0.2	1.1 ± 0.1	1.44 ± 0.3
δ (μm^{-1})	0.41	0.71	0.93	1.7	1.4	5.2	15.0

ficients confirmed the assumed exponential depth dependence of the concentration. The δ values associated with soft-segment bands were much smaller than that of the hard-segment band, indicating that chemical degradation occurred selectively in the soft segment. The δ values associated with the linkage region, such as the non-hydrogen-bonded urethane carbonyl at 1730 cm^{-1} and the hydrogen-bonded urethane carbonyl at 1709 cm^{-1} were intermediate between the values of the soft and the hard segments. The higher δ-value of the band at 1709 cm^{-1} relative to the one at 1730 cm^{-1} reflected the lower reactivity of the hydrogen-bonded urethane.

The δ-values were used to calculate the relative concentration profiles from eq. (2). The profiles for some functional groups from the soft segment, the linkage region, and the hard segment are plotted in Figure 5. The relative concentrations of groups from the soft segment (curves a and b) approached unity about 6–10 microns from the surface. Although the soft segment was affected to a depth up to 10 microns, the affected depth of the hard segment was at most less than 0.5 microns (curve d), an indication that the hard segment was essentially undegraded. The affected depth of the linkage region was between the soft segment and the hard segment, around 2–4 microns (curve c). Figure 5 shows the depth profiles in the most cloudy area. The affected depths varied from one region to another since the implanted sample surfaces were heterogeneous.

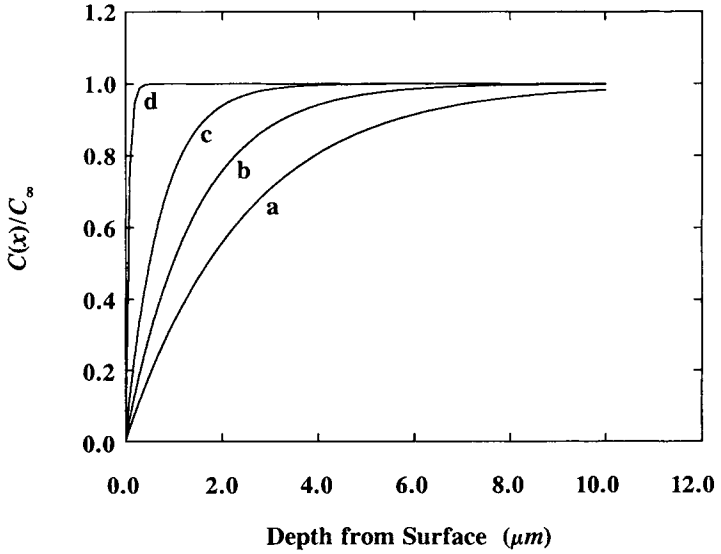

Figure 5 Relative concentration profiles in a cloudy area of implanted Sample A: (a) 2791 cm^{-1} CH_2; (b) 1364 cm^{-1} CH_2; (c) 1730 cm^{-1} nonhydrogen-bonded urethane carbonyl; (d) 1219 cm^{-1} amide III from urea and urethane.

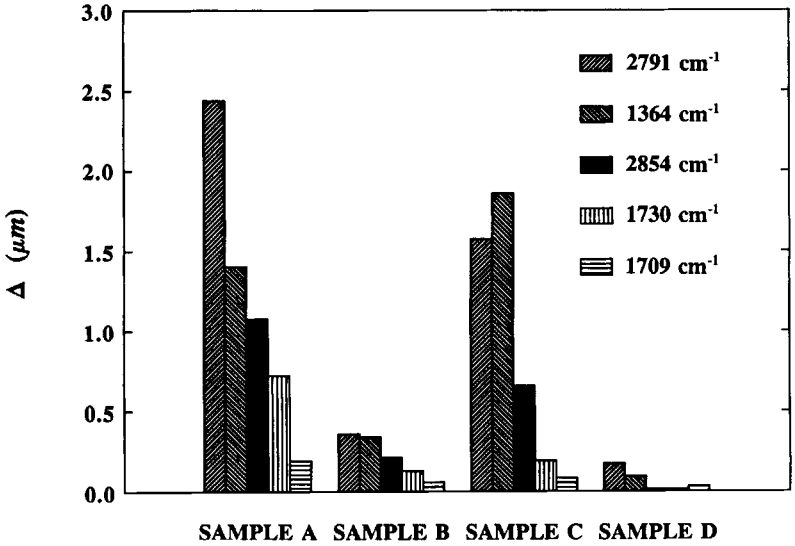

Figure 6 Comparison of degradation depths in the most cloudy areas of different PEU samples after 10 weeks implantation.

Probe of Degradation Mechanism

To evaluate the effect of stabilizers, a characteristic depth of degradation, Δ, was defined as the depth at which $C(x)/C_\infty = 1 - e^{-1}$. By this definition,

$$\Delta = \frac{1}{\delta} \tag{8}$$

Figure 6 compares the characteristic depth in the most cloudy areas of the different PEU samples after 10 weeks implantation. The bands shown here were from the soft segment and the linkage region. The degradation was greatly diminished by addition of Santowhite (Sample B), while Methacrol (Sample C) had less effect, probably because it leached out during implantation. When both Santowhite and Methacrol were added (Sample D), the degradation was the least. Santowhite and Methacrol are both antioxidants, and their effectiveness in suppressing degradation suggested that the chemical changes to the PEU were oxidative in nature.

Since degradation occurred preferentially in the soft segment, it was desirable to locate the site of attack in the soft segment. Figure 7 shows the 3000–2700 cm^{-1} region of the infrared spectrum that is associated with the methylene groups of the PTMEG soft segment. The soft segment is characterized by two different methylenes: α- and β-methylenes:

$$\underset{\alpha\ \ \beta\ \ \beta\ \ \alpha}{-(O-CH_2CH_2CH_2CH_2)_n-O-}$$

The α-methylene absorbs at 2791 cm^{-1}, whereas the β-methylene has a distinct band at 2940 cm^{-1}. The band at 2854 cm^{-1} is the combined vibrations of the α- and β-methylenes.[17] The Δ-values associated with

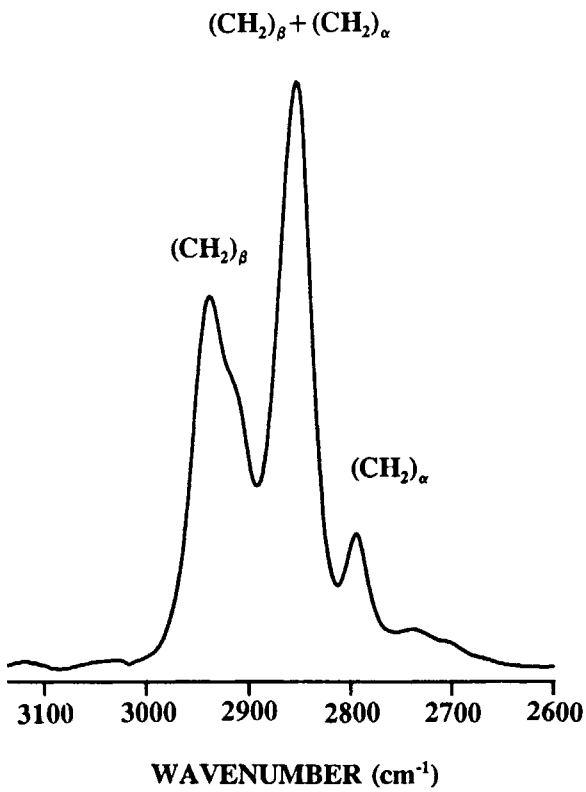

Figure 7 Methylene bands in the 3000–2700 cm^{-1} region.

Table III Δ Values of the Three Methylene Bands in the Cloudy Areas of Different Samples after 10 Weeks Implantation

Band (cm^{-1})	Assignment[17]	Sample A (μm)	Sample B (μm)	Sample C (μm)	Sample D (μm)
2940	$\nu_a(C-H)_\beta$	0.58	0.09	0.26	0.04
2854	$\nu_s(C-H)_\beta + \nu_a(C-H)_\alpha$	1.1	0.21	0.66	0.08
2791	$\nu_s(C-H)_\alpha$	2.4	0.36	1.6	0.17

the three methylene bands of implanted PEU samples are listed in Table III. The band at 2791 cm^{-1} possessed the highest value of Δ, whereas the band at 2940 cm^{-1} had a Δ-value only $\frac{1}{5}$ to $\frac{1}{4}$ that of the 2791 cm^{-1} band. This suggested that degradation occurred selectively at the α-methylene, i.e., the methylene linked to the ether group. The Δ-values from Samples B, C, and D, though the magnitudes differed due to the effect of stabilizers, displayed the same order for the three methylene absorptions, i.e., the Δ-value was largest for the 2791 cm^{-1} band and smallest for the 2940 cm^{-1} band in all cases.

Consistent with an oxidative degradation mechanism, the *in vivo* degradation of PEUs produced numerous new IR bands that were identified as carboxylic acid and alcohol groups. The new bands were also analyzed to obtain the concentration profiles. In this case, the concentration decreased from the surface inward and was assumed to follow an exponential relationship of the form

$$C(x) = C_0 e^{-\delta' x} \tag{9}$$

where C_0 is the concentration at the surface, and δ', similar to δ, is a parameter that reflects the rate of the concentration change. The analogous expression to eq. (6) is

$$\left(\frac{A}{A_r}\right)^{-1} = \frac{1}{K'} + \frac{\delta'}{2K'} d_p \tag{10}$$

where $K' = (d_e \epsilon C_0)/(d_e \epsilon \mathbf{C})_r$. The parameters K' and δ' are obtained from experimental data.

Since most of the new bands appeared as shoulders, it was necessary to deconvolute them. However, either due to the complexity of the overlapping peaks or their low intensities, it was not possible to obtain quantitative absorbance values for most of the new bands. Table IV lists the K' and δ' values for two of the new bands, the $-CO-O-$ stretching at 1174 cm^{-1} and the $C-OH$ stretching at 1255 cm^{-1}, in Sample A that were obtained by deconvolution of the peaks in the region 1270–1150 cm^{-1}. Using the δ' values, the relative concentration profiles were calculated by eq. (9) and are plotted in Figure 8. By comparing with Figure 5, it is noted that the depth range in which these new bands appeared was similar to the range in which the soft-segment bands decreased, suggesting that the degradation products were derived from the reaction of the soft segment.

Proposed Degradation Mechanism

It has been demonstrated that PEU *in vivo* degradation took place essentially in the soft segment at the ether linkage of the PTMEG chains. The degradation resulted in the production of carboxylic acid and alcohol groups. Based on these experimental observations and the fact that antioxidants reduced the degradation, an oxidative degradation mechanism was proposed for the *in vivo* degradation of PEUs (Fig. 9). It is known that macrophages quickly adhere to the implanted polymer surface, become activated, and form foreign body giant cells.[5] A previous investigation[5] also showed that the cracked areas followed directly from coverage and activation of foreign body giant cells. The activated cells release superoxide anion radicals and enzymes[24] and change the interfacial environment into the acidic range.[25] The superoxide anion radicals combine with protons rapidly to form hydroperoxide radicals. It is proposed that the oxidative species, the hydroperoxide radical, then attacks the α-carbon of the PEU soft segment and subsequently oxidizes it to an ester linkage. This results in the large decrease in ether bands in the

Table IV δ Values of Two New Bands in the Cloudy Area of Implanted Sample A

Band (cm^{-1})	1174	1255
Linear regression coefficient	0.949	0.850
K	1.9	3.0
δ (μm^{-1})	0.75	0.51

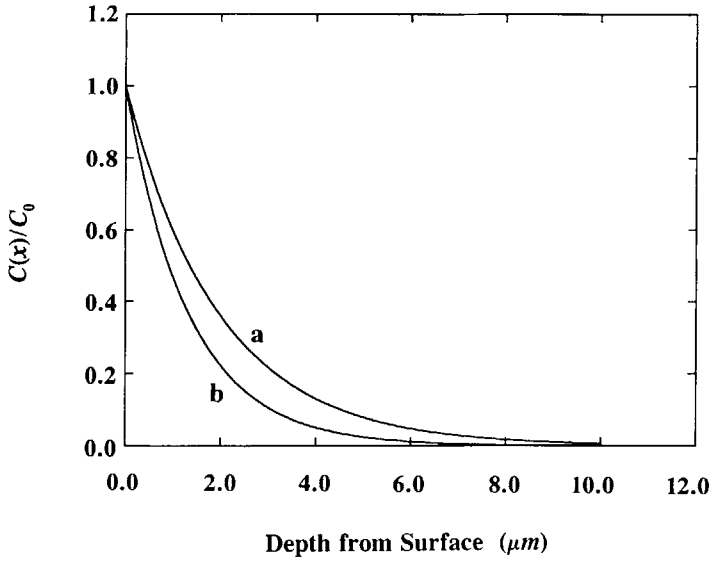

Figure 8 Relative concentration profiles for two of the new bands in the cloudy area of implanted Sample A: (a) 1255 cm^{-1} hydroxyl; (b) 1174 cm^{-1} carboxylic acid.

ATR–IR spectra, for example, the band at 2791 cm^{-1}. It has previously been observed that an ester group is formed by attack of a hydroperoxide radical on an ether group.[26] The ester group is not stable in the presence of esterases[27] or acid that can hydrolyze the ester to a carboxylic acid and an alcohol. The polyether segment may undergo further depolymerization from the free end in the acidic environment,[28] causing a greater loss of soft segment. The loss of soft segment could produce embrittled areas on the surface and subsequently cause the microcracking that appeared as cloudy areas when viewed at the macrolevel in the optical microscope.

CONCLUSIONS

Chemical changes associated with the surface cracking of cage-implanted PEU films have been characterized with the micro-ATR–FTIR technique. Analysis of spectral features led to the following conclusions:

1. Chemical degradation was found in areas that appeared cloudy in the optical microscope, whereas no significant changes were observed in the clear areas of PEU samples implanted for 10 weeks.
2. The concentration profiles in the depth direction followed an exponential form; the affected depth was as much as 10 microns.
3. The degradation occurred preferentially in the soft-segment region at the α-carbon adjacent to the ether group; the degradation products included carboxylic acid and alcohol groups.

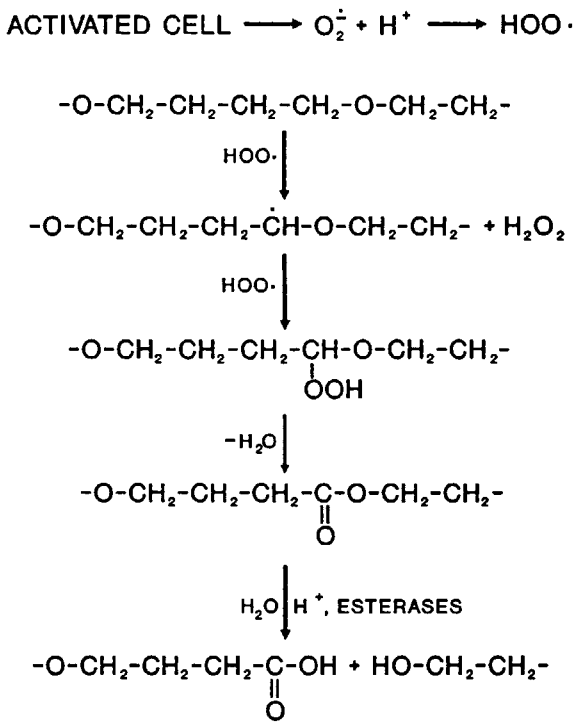

Figure 9 A proposed mechanism for *in vivo* degradation of PEU.

4. Antioxidant stabilizers effectively reduced the amount of degradation, consistent with an oxidative degradation mechanism.
5. An oxidative degradation mechanism was proposed that started with cell adhesion and activation, followed by release of oxidative agents that attacked the polymer.

This work was generously supported by the E. I. du Pont Company and the National Institutes of Health, grant number HL 25239.

REFERENCES

1. H. E. Kambic, S. Murabayashi, and Y. Nosè, *C&EN*, **April 14,** 31 (1986).
2. J. W. Boretos, in *Polyurethanes in Biomedical Engineering,* H. Plank, G. Egbers, and I. Syre, Eds., Elsevier, Amsterdam, 1984, p. 135.
3. K. Stokes, P. Urbanski, and J. Upton, *J. Biomater. Sci. Polym. Ed.,* **1,** 207 (1990).
4. Y. Wu, Q. Zhao, J. M. Anderson, A. Hiltner, G. A. Lodoen, and C. R. Payet, *J. Biomed. Mater. Res.,* **25,** 725 (1991).
5. Q. Zhao, N. Topham, J. M. Anderson, A. Hiltner, G. A. Lodoen, and C. R. Payet, *J. Biomed. Mater. Res.,* **25,** 177 (1991).
6. K. B. Stokes, *J. Biomater. Appl.,* **3,** 228 (1988).
7. H. Ishihara, I. Kimura, K. Saito, and H. Ono, *J. Macromol. Sci.-Phys.,* **B10,** 591 (1974).
8. V. W. Srichatrapimuk and S. L. Cooper, *J. Macromol. Sci.-Phys.,* **B15,** 267 (1978).
9. D. O. Hummel, G. Ellinghorst, A. Khatchatryan, and H. D. Stenzenberger, *Angew. Makromol. Chem.,* **82,** 129 (1979).
10. C. S. P. Sung and C. B. Hu, *Macromolecules,* **8,** 68 (1975).
11. C. S. P. Sung and C. B. Hu, *J. Biomed. Mater. Res.,* **12,** 791 (1978).
12. R. Iwamoto, K. Ohta, T. Matsuda, and K. Imachi, *J. Biomed. Mater. Res.,* **20,** 507 (1986).
13. P. M. Bummer and K. Knutson, *Macromolecules,* **23,** 4357 (1990).
14. S. I. Stupp, J. W. Kauffmen, and S. H. Carr, *J. Biomed. Mater. Res.,* **11,** 237 (1977).
15. T. J. Lenk, B. D. Ratner, R. M. Gendreau, and K. K. Chittur, *J. Biomed. Mater. Res.,* **23,** 549 (1989).
16. M. K. Antoon, J. K. Koenig, and J. L. Koenig, *Appl. Spectrosc.,* **31,** 518 (1977).
17. H. Tadokoro, A. Umehara, and S. Murahashi, *J. Chem. Phys.,* **24,** 2807 (1965).
18. G. Socrates, *Infrared Characteristic Group Frequencies,* Wiley, Chichester, 1980.
19. L. J. Bellamy, *The Infrared Spectra of Complex Molecules,* Chapman and Hall, London, 1985, Vol. 1.
20. K. Knutson, and D. J. Lyman, in *Surface and Interfacial Aspects of Biomedical Polymers,* J. D. Andrade, Ed., Plenum, New York, 1985, Vol. 1, Chap. 6.
21. N. J. Harrick, *J. Opt. Soc. Am.,* **55,** 851 (1965).
22. H. G. Tompkins, *Appl. Spectrosc.,* **28,** 335 (1974).
23. D. J. Carlsson and D. M. Wiles, *Can. J. Chem.,* **48,** 2397 (1970).
24. I. Fridovich, in *Oxygen Radicals and Tissue Injury,* B. Halliwell Ed., Federation of American Societies of Experimental Biology, Bethesda, MD, 1988, p 1.
25. I. A. Silver, R. Murrills, and D. J. Etherington, *Exp. Cell Res.,* **175,** 266 (1988).
26. A. Robertson, *Nature,* **162,** 153 (1948).
27. A. M. Reed and D. K. Gilding, *Polymer,* **22,** 494 (1981).
28. P. Dreyfuss, M. P. Dreyfuss, and G. Pruckmayer, in *Encyclopedia of Polymer Science and Engineering,* H. F. Mark et al., Eds., Wiley, New York, 1989, Vol. 16.

Received September 10, 1991
Accepted October 10, 1991